Energy Harvesting Techniques for Health Monitoring and Indicators for Control of a Damaged Pipe Structure

Paul Cahill[1], Vikram Pakrashi[2,*], Peng Sun[3], Alan Mathewson[4], Satish Nagarajaiah[3,5]

[1]*MaREI Centre, Environmental Research Institute, Beaufort Building, University College Cork, Haulbowline Road, Ringaskiddy, Co. Cork, Ireland.*
[2]*Dynamical Systems and Risk Laboratory, School of Mechanical and Materials Engineering, University College Dublin, Belfield, Dublin 4, Ireland.*
[3]*Department of Civil and Environmental Engineering, Rice University, Houston, TX 77005, USA.*
[4]*Micro & Nano Systems Centre, Tyndall National Institute, University College Cork, Dyke Parade, Cork, Ireland.*
[5]*Department of Mechanical Engineering and Department of Material Science and Nano-Engineering, Rice University, Houston, TX 77005, USA.*

(Received keep as blank , Revised keep as blank , Accepted keep as blank)

Abstract. Applications of energy harvesting from mechanical vibrations is becoming popular but the full potential of such applications is yet to be explored. This paper addresses this issue by considering an application of energy harvesting for the dual objective of serving as an indicator of structural health monitoring (SHM) and extent of control. Variation of harvested energy from an undamaged baseline is employed for this purpose and the concept is illustrated by implementing it for active vibrations of a pipe structure. Theoretical and experimental analyses are carried out to determine the energy harvesting potential from undamaged and damaged conditions. The use of energy harvesting as indicator for control is subsequently investigated, considering the effect of the introduction of a tuned mass damper (TMD). It is found that energy harvesting can be used for the detection and monitoring of the location and magnitude of damage occurring within a pipe structure. Additionally, the harvested energy acts as an indicator of the extent of reduction of vibration of pipes when a TMD is attached. This paper extends the range of applications of energy harvesting devices for the monitoring of built infrastructure and illustrates the vast potential of energy harvesters as smart sensors.

Keywords: energy harvesting; piezoelectric; structural health monitoring; passive control; pipes; damage; experimental analysis

1. Introduction

The design and optimization of piezoelectric based energy harvesting devices has received significant attention in recent times, with a wide range of potential applications having been identified (Saadon and Sidek 2011). Such devices are based on the principle of piezoelectric materials having the ability to convert fluctuations in strain experienced by the material into electrical energy (Erturk and Inman 2011). When such devices are bonded to a host structure, the amount of electrical energy which is generated by the material will be an indication of the dynamic strain conditions that the host structure undergoes (Chen and Wang 2004). A change in such strain conditions due to damage within the host will therefore be reflected by the change in the output of

*Corresponding Author: vikram.pakrashi@ucd.ie

electrical energy produced by the material when the structure is subjected to dynamic loading conditions (Cahill et al. 2014a). Additionally, as the electrical output is dependent on the strain conditions of the host structure, there is the potential for monitoring loadings conditions which produce such dynamical responses of the host structure (Kim et al. 2011). The question thereby arises as to the potential applications of piezoelectric based energy harvesting devices for use with civil infrastructure elements, with structures included bridge structures (Cahill et al. 2016), individual elements such as reinforced concrete beams (Cahill et al. 2014b) and traffic vehicles (Amoroso et al. 2015). By monitoring the output of energy harvesters, it can become possible to detect the presence of damage through variations in the electrical energy output and act as an indicator for control of the host structure.

The modelling and response of damaged and undamaged cantilever beams undergoing free and forced vibrations is well known (Jassim et al. 2013). This has been a popular model to test methodologies utilized for SHM (Carden and Fanning 2004). Detection of damage through the changes in natural frequency of the structure has been shown through finite element analysis and experimental testing of a damaged cantilever structure (Nahvi and Jabbari 2005) in this regard. On the other hand, a range of other detection methods have been developed for application in built infrastructure (Jaksic et al. 2016; Pakrashi et al. 2013). The use of piezoelectric energy harvesting sensors to monitor damage evolution within a pipe structure undergoing impact based loading has been proposed through the analysis of the generated voltage signal using Fourier and wavelet based analysis (Cheraghi et al. 2005). The use of empirical mode decomposition utilizing piezoelectric sensor outputs from a damaged pipe structure has also been proposed for damage detection of the host structure (Rezaei and Taheri 2009), as has piezoelectric impedance-based monitoring (Park et al. 2003). The use of fluid pressure waves for the detection of leaks using piezoelectric materials has also been investigated as a damage detection method for pipe based structures (Taghvaei et al. 2007).

While SHM techniques have become more popular over time, implementation of vibration control technologies to structures has simultaneously become mature over time (Nagarajaiah and Jung 2014). Use of passive control devices like tuned mass dampers (TMDs) (Nagarajaiah 2009) is one of such technologies. TMDs can be optimized for an individual structure (Marano et al. 2008) and through the use of tracking algorithms, TMDs can be tuned to account for changes to the natural frequency of the host structure (Arrigan et al. 2011; Arrigan et al. 2014; Pasala and Nagarajaiah 2014; Contreras et al. 2014; Jang et al. 2014). Multiple smart TMDs have also been considered in this regard (Sun et al. 2014). The adaptation of smart materials with vibration control has also received attention including the coupling of an electro-magnetic harvester with TMDs (Gonzalez-Buelga et al. 2014), in recent times. Piezoelectric materials have been used as actuators for the control of vibrations for a cantilever pipe, whereby voltage is applied to the material to induce a strain response, which in turn introduces damping to the host pipe structure (Song et al. 2006). While these studies have proposed energy harvesting devices coupled with civil infrastructure for different applications, the use of piezoelectric energy harvesters as a means to detect adverse vibrations in the host structure and indicate the requirement for control or estimate the level of control systems already in place is yet to be established. Additionally, estimating such harvesting values efficiently can also lead to an integration with adaptive algorithms for energy hungry sensors (Srbinovski et al. 2016).

This paper partly addresses this gap and investigates the use of piezoelectric energy harvesters to act as damage detectors and indicators for control through the analysis of the voltage response and power output of the harvesters using simulations and laboratory experiments. A cantilever pipe structure is investigated, for undamaged and damaged conditions. Energy harvesting for forced

vibration of this cantilever pipe is subsequently estimated, with the undamaged energy harvesting estimates from the structure compared against that for a damaged condition. The use of such energy harvesters as indicators for control is subsequently investigated for a TMD connected to the pipe. Numerical studies are compared with experimental results and the work is expected to create a benchmark evidence base for utilizing energy harvesting as an indicator for structural health and control.

2. Modelling of Energy Harvesting Device and Host Pipe Structure

2.1 Piezoelectric Energy Harvesting Device

The behavior of piezoelectric materials can be expressed through the linear fundamental relationships which were formalized by the Institute of Electrical and Electronics Engineers (IEEE), and is represented as (IEEE 1988):

$$S_p = s_{pq}^E T_q + d_{kp} E_k \tag{1}$$

and

$$D_i = d_{iq} T_q + \varepsilon_{ik}^T E_k \tag{2}$$

where S is the strain vector, D is the electric displacement vector, s^E is the elastic compliance matrix under constant electric field, denoted by E, d is a piezoelectric constant matric, ε^T is the permittivity matrix under constant stress, denoted by ^{T}. The superscripts T and E are the stress and electric field matrix respectively. These fundamental relationships can be used to establish the response of piezoelectric materials which are subjected to strain fluctuations and in determining the subsequent electric response. Such a response is named the direct piezoelectric effect, whereas the strain response of a material due to an applied electric field is known as the indirect piezoelectric effect (Sodano *et al. 2016*), which can similarly be determined from the fundamental relationships.

Fig. 1 Example of piezoelectric energy harvester bonded to surface of host structure

A patch based piezoelectric energy harvester is designed so as to be bonded directly to the surface of the host structure, thus converting surface strain fluctuations of the host into electrical energy (Fig. 1). The voltage response of such a harvester when undergoing dynamic applied strain due to vibrations of the host structure has recently been formulated (Sirohi and Chopra 2000; Erturk 2011) and can be expressed as:

$$\frac{dv(t)}{dt} + \frac{v(t)}{\tau} = \frac{e_{31}A}{C_p}\frac{d}{dt}\left[S_1(t) + S_2(t)\right] \tag{3}$$

where v is the voltage, τ and e_{31} are a time and piezoelectric constant, respectively, and A and C_p are the area and capacitance of the material. The strain fluctuations, with respect to time, for the two principal directions are given by S1 and S2 for the longitudinal and translational directions of the material respectively. τ is given as $\tau = C_p R_l$, where R_l is the external resistive load and the capacitance of the piezoelectric material can be calculated by

$$C_p = \frac{\varepsilon_{33}^S A}{t_m} \tag{4}$$

where ϵ_{33}^S is the permittivity at constant strain of the material and t_m is the thickness. The power output, P, from the material under fluctuating strain can finally be determined through

$$P = \frac{\left(\sqrt{\frac{1}{T}\int_0^T v^2(t)dt}\right)^2}{R_l} \tag{5}$$

where T is the total time period considered. The transfer of energy through the bond layer, i.e. from the surfaces of the host structure to the piezoelectric material, is taken as being linear (Rabinovitch and Vinson 2002), which results in no losses in the transfer of strain energy between the two.

2.2 Modelling of Host Structure

The host structure considered in this study is a steel pipe structure. To understand how energy harvesting can act as an indicator for SHM, the energy harvesting potential from the healthy condition of this steel pipe must first be determined, so as to provide a baseline. The host steel pipe was modelled as an Euler Bernoulli cantilever beam of length L and circular cross-section, subject to forced vibrations in the form of sinusoidal loadings of varying frequencies and magnitudes (Fig. 2(a)). The equation of motion of the pipe is

$$EI\frac{\partial^4 y(x,t)}{\partial x^4} + \rho\bar{A}\frac{\partial^2 y(x,t)}{\partial t^2} + c\frac{\partial y(x,t)}{\partial t} = F_p \sin(\omega t)\,\delta(x - x_P) \tag{6}$$

where E and I are the modulus of elasticity of the material of the beam and second moment of area of the cross-section of the beam respectively, ρ is the density of the beam, $\bar{A}$ is the cross-sectional area of the beam and c is the equivalent viscous damping of the beam. The response of the beam relative to its neutral position at a location x away from the left hand support at time t is given as $y(x,t)$, where ∂ is the partial derivative operator. The applied excitation force, applied at a distance of x_P along the length of the beam from the fixed support, is given by F_P at a loading frequency of ω, with δ being the Dirac delta function.

In order to investigate the feasibility of using energy harvesting devices to act as an indicator for control, this baseline model is considered coupled with a TMD, which is represented as a single degree of freedom (SDOF) system (Fig. 2(b)). The equation of motion of the beam following the inclusion of a TMD is

$$EI\frac{\partial^4 y(x,t)}{\partial x^4}+\rho\bar{A}\frac{\partial^2 y(x,t)}{\partial t^2}+c\frac{\partial y(x,t)}{\partial t}=F_p\sin(\omega t)\,\delta(x-x_P)-m_{TMD}\frac{\partial^2 z_1}{\partial t^2}\delta(x-x_1) \quad (7)$$

where m_{TMD} is the mass of the TMD and k_{TMD} and c_{TMD} being the stiffness and damping respectively. The response of the TMD relative to the static deflection at the location at which the TMD is attached to the beam, a distance x_1 from the fixed support, is given by z_1. The response of the TMD when coupled with the host structure is

$$m_{TMD}\frac{\partial^2 z_1}{\partial t^2}+c_{TMD}\frac{\partial z_1}{\partial t}+k_{TMD}z_1=m_{TMD}\frac{\partial^2 y(x_1,t)}{\partial t^2} \quad (8)$$

where $y(x_1,t)$ is the response of the beam where the TMD is located and the right hand side of Equation 8 is the base excitation of the TMD. Considering separation of variables and the orthogonality of mode shapes for the beam, the equations of motions can be written as

$$[M]\{\ddot{q}(t)\}+[C]\{\dot{q}(t)\}+[K]\{q(t)\}=\{R(t)\} \quad (9)$$

where *[M]* is the mass matrix, *[C]* is the damping matrix and *[K]* is the stiffness matrix of the structure, *q(t)*, $\dot{q}(t)$ and $\ddot{q}(t)$ are the modal displacement, velocity and accelerations respectively and *R(t)* is the load vector vectors respectively. The over-dots denote differentiation with respect to time.

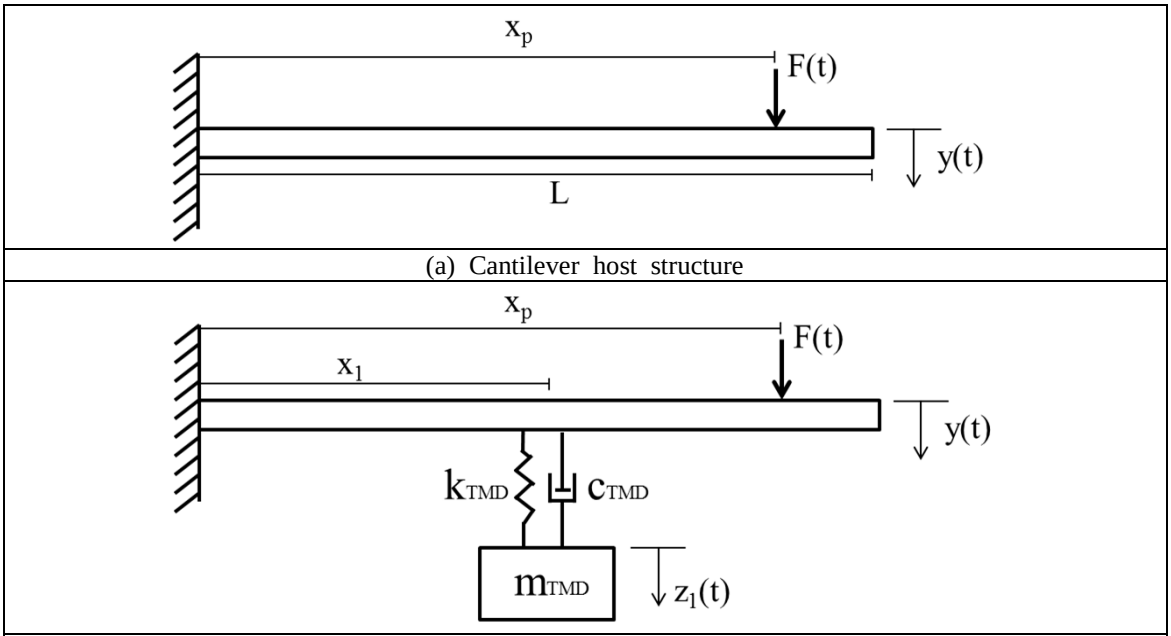

(a) Cantilever host structure

(b) Combined dynamical system

Fig. 2 Illustrations of host structure with (a) Host structure under forced vibrations (b) Combined dynamical system with primary cantilever structure and coupled tuned mass damper

2.3 Assembly of Host Structure Models

To determine the applications related to the use of energy harvesting devices with the host pipeline structure, an investigation was performed to determine the suitability of the host model type for the purposes of energy harvesting applications. In this regard, a comparison of two types of models was performed using Strand7, Finite Element Software, namely a beam model and solid brick model. The comparison of the beam and brick models ensures that the dynamical behavior of the structure is accurately achieved for a range of scenarios, including the influence of the introduction and evolution of damage and the influence of coupling control mechanisms on the host. This ensures that the applications arising from the introduction of energy harvesters to the structure as investigated in this study are captured to a satisfactory degree of accuracy, including power generation, damage detection and control indication. The two models were created for the same geometric and material properties so as to model a steel cantilever beam structure, with a hollow circular cross-section. The geometric and material properties as employed for both models are presented in Table 1.

Table 1. Geometric and material properties of host cantilever pipe structure

Parameter	Symbol	Value	Unit
Length	L	4.725	M
Inner Radius	r_i	0.03187	M
Outer Radius	r_o	0.03667	M
Young's Modulus	E	200	GPa
Density	ρ	7850	kg/m^3
Moment of Inertia	I	6.094×10^{-7}	m^4

The beam model was constructed using a total of 3780 beam elements, which encompass axial, bending and torsional stiffness. With an overall length of 4.725m, each element was assigned uniform cross-sectional geometry and material properties including density and Young's Modulus. To model the fixed boundary conditions of a cantilever structure, the boundary conditions of the first node was restrained for both translation and rotation. With the introduction of applied load to provide external excitation to the model, the dynamic response of the structure can be ascertained and the energy harvesting potential from the introduction of energy harvesting devices can be determined. The solid brick model was created using 4-Node tetrahedral (Tet4) elements, consisting of four nodes each with three translational degrees of freedom. The solid elements enable rotation of the faces of the element through relative translations at the nodes. Through predefining the geometric properties of the desired host structure, automeshing functions allowed for the creation of the solid brick model. A line mesh was generated using the geometric properties and vertices were placed at locations requiring a high resolution mesh density, such as at the end of the structure, and at intervals of 0.08m along the length of the host. A surface mesh was subsequently created using Quad4 plate elements and following mesh cleaning, a solid mesh model was created using the Tet4 brick elements. As with the beam model, the boundary conditions of the nodes located at the fixed end of the beam were restrained for translation and rotation, and the material properties of the solid elements assigned as per Table 1.

Following the assembly of the beam model and solid brick model, a comparison of both was completed. It was found that both models agreed to a reasonable degree of accuracy, with the first mode of beam model being 3.068Hz, compared to 3.095Hz for the solid brick model. The second

and third modes were found to be 19.237*Hz* and 53.864*Hz* for the beam model, respectively, with the solid brick model having a second mode of 19.35*Hz* and a third mode of 54.005*Hz*. The response of the models was also compared under external excitation, with identical loading conditions being applied through a sinusoidal load of 25*N* being employed at a distance of 0.5*m* from the fixed end of both model. The dynamic responses, including displacement, velocity and acceleration, of the models were found to be in good agreement, with the beam model having a peak displacement of 14.44*mm* and the solid model having a peak displacement of 14.20*mm* (Fig. 3).

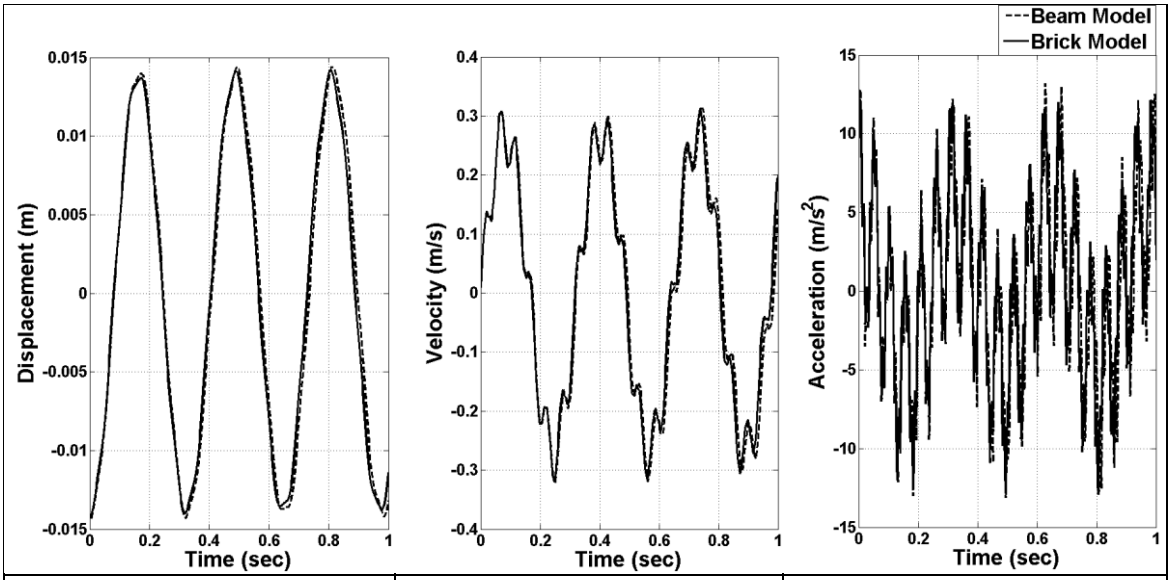

(a) Model displacements | (b) Model velocities | (c) Model accelerations

Fig. 3 Comparison of dynamical response at mid-span of beam model and brick models under identical loading conditions for (a) Displacement (b) Velocity and (c) Acceleration

Following this, the effects of the introduction and evolution of damage was investigated for both models, with two damage cases being considered to ensure dynamical similitude. The first case considered is the manifestation of damage, in the form of open cracks, of width, height and depth 2.5*mm*, 35.5*mm* and 4.58*mm* respectively, located on opposing sides of the pipe at a distance of 1.89*m* along the length of the pipeline structure. The second damage case considered was damage consistent with that of the first case, in conjunction with a second, additional location of damage. The second location of damage had a magnitude of damage equal in magnitude to that of the damage at the first location and was introduced at a location of 2.98*m* along the length of the beam.

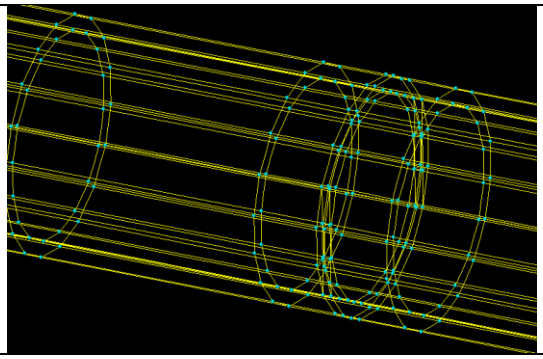

(a) Line mesh created with vertices positioned along length of the beam and at location of damage

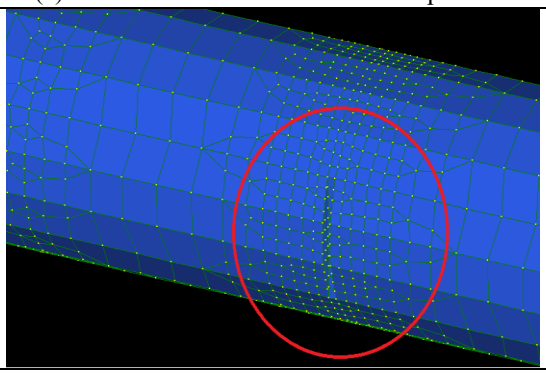

(b) Resultant surface mesh with location of damage highlighted

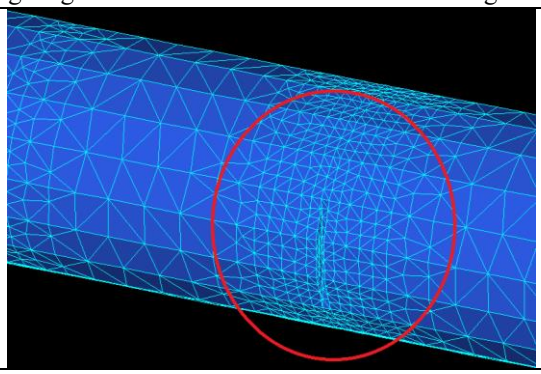

(c) Final brick model with location of damage highlighted

Fig. 4 Creation of brick element model with line mesh, surface mesh and resultant brick model with location of damage highlighted

Table 2. Natural frequencies of beam and brick models for undamaged, damage case 1 and damage case 2

	Beam Model			Brick Model		
	Undamaged	Dam. I	Dam II.	Undamaged	Dam. I	Dam II.
1st Mode	3.069	3.069	3.069	3.095	3.093	3.093
2nd Mode	19.237	19.237	19.235	19.350	19.331	19.307
3rd Mode	53.864	53.863	53.861	54.005	53.971	53.902

The influence of the introduction of the two damage cases on the beam and solid brick model and, therefore, the ability of the models to accurately represent damage effects were subsequently compared. It was found that The influence of the damage both at one and at two locations was found to have little effect on the global natural frequency at the first mode for the beam element model, while the brick element model displays a reduction from 3.095*Hz* to 3.093*Hz* (Table 2). It can be seen, however, in the subsequent modes that the influence of damage does register, with the second mode of the beam model reducing from 19.237*Hz* to 19.235*Hz* and the third mode decreasing from 53.864*Hz* to 53.861*Hz* from undamaged to damage case 2. The influence of damage was found to have a marginal influence on the first mode of the solid brick model, with a reduction in frequency of 0.002*Hz*. The second mode showed a larger decrease, from 19.35*Hz* undamaged to 19.307*Hz* for the second damage case, whilst the third mode decreased from 54.005*Hz* to 53.903*Hz* respectively. These results

illustrate that the use of a beam element model is valid for the introduction of damage through the reduction of the flexural rigidity at the damage location and is suitable to use for investigating the applications that arise from introducing energy harvesting devices to the host pipeline structure.

3. Energy Harvesting from Host Structure

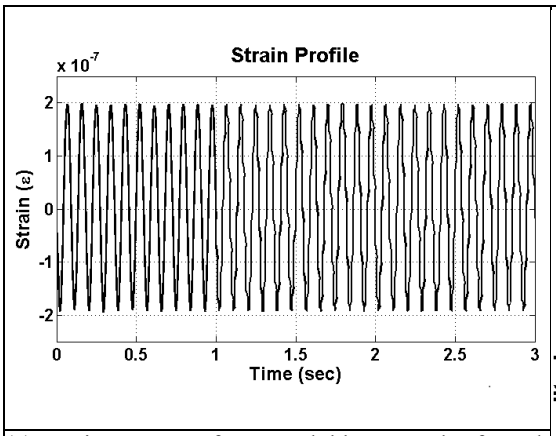

(a) Strain response from model beam under forced vibration

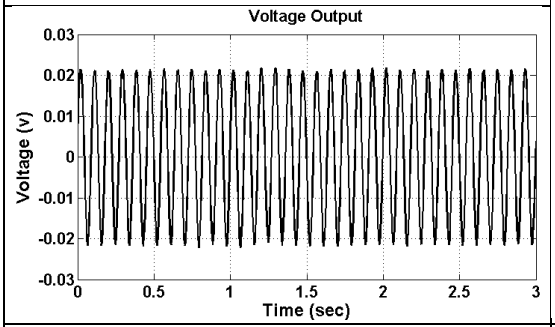

(b) Voltage output from energy harvester

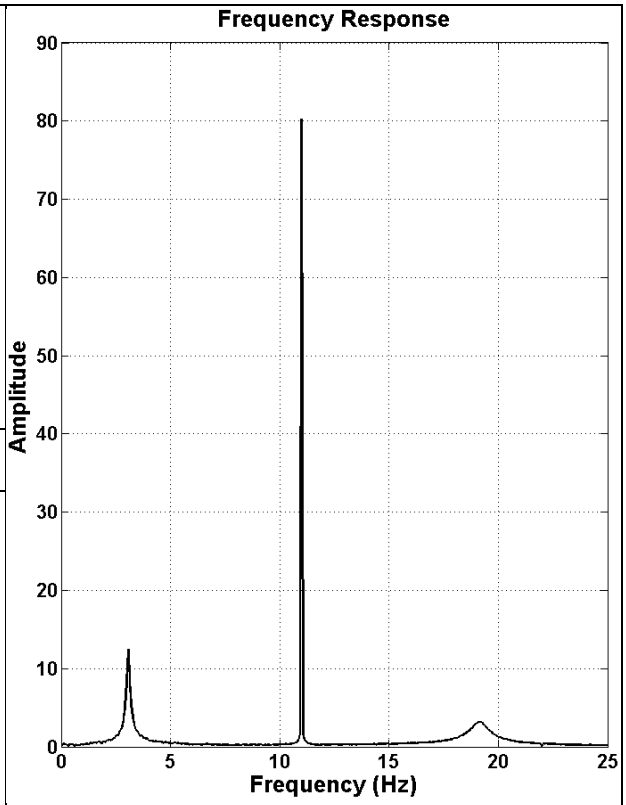

(c) Frequency response of energy harvester

Fig. 5 Illustration of sample (a) Strain profile of beam undergoing forced vibration (b) Resultant voltage output from energy harvester and (c) Frequency response of energy harvester

For the use of piezoelectric based energy harvesters to act as damage detectors and indicators for control it is first necessary to establish a power output baseline for the healthy host structure as a marker. To determine the energy harvesting potential from the baseline case, a loading parameter study was completed with sinusoidal loading of $25N$, of frequencies between $3Hz$ and $27Hz$, being applied at three locations along the beam, namely $x_p = 0.5m$, $x_p = 1.182m$ (quarter-span) and $x_p = 2.361m$ (mid-span). Energy harvesting devices were modelled at fourteen locations along the length of the beam, at spacing of $0.5m$ as well as at the mid and quarter spans and the locations at which damage is to be introduced. The calculation of the power output at these locations was determined for each of the loading cases, with the properties of the piezoelectric energy harvesting device, based on Lead Zirconate Titanate (PZT) material, given in Table 3.

Table 3. Properties of piezoelectric material for energy harvesting device

Parameter	Symbol	Value	Unit
Piezoelectric Charge Constant	d_{31}	-190×10^{-12}	C/m
Capacitance	C_p	95	n/F
Piezoelectric Constant	e_{31}	-8.55	C/m^2
Length of Piezoelectric Material	l_m	0.05	M
Breadth of Piezoelectric Material	b_m	0.025	m
External Resistive Load	R_l	1000	$k\Omega$

Any damping effects as a result of the energy harvesting devices are excluded, as the mass of the active piezoelectric material is insignificant against the mass of the structure and as such will not influence the response. An example response from an energy harvester is shown for a loading frequency of 11Hz, with the strain profile, resultant voltage output and frequency response shown (Fig. 5).

3.1 Influence of Loading Frequency on Energy Harvesting Potential

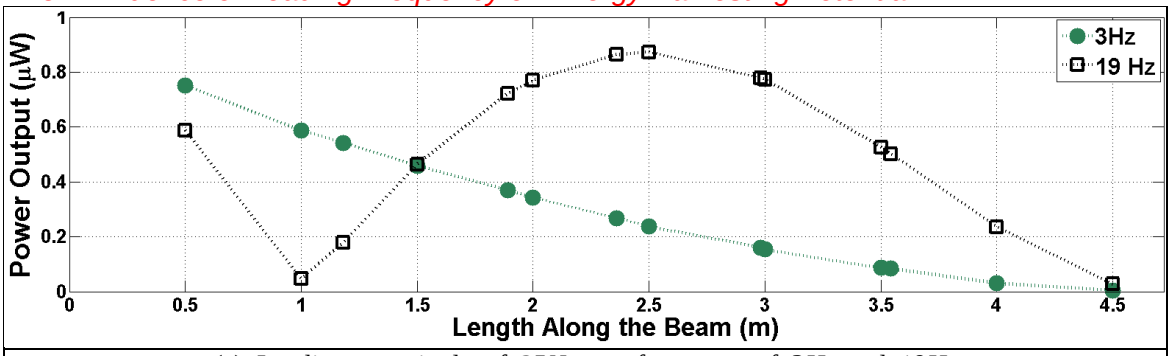

(a) Loading magnitude of 25N at a frequency of 3Hz and 19Hz

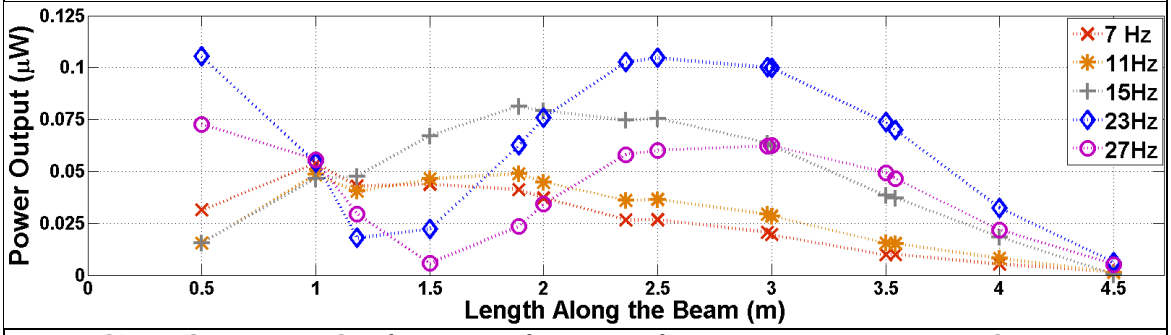

(b) Loading magnitude of 25N at a frequency of 7Hz, 11Hz, 15Hz, 23Hz and 27Hz

Fig. 6 Energy harvesting potential from host beam at loading magnitude of 25N at various loading frequencies

The energy harvesting potential from the host beam for a 25N load being applied at $x_p = 0.5m$ at a range of frequencies was determined. The application of loading close to the first and second natural frequency of the beam produced the highest magnitude of power output from the energy

harvesters (Fig. 6(a)). The peak power output from the beam was found to be $0.873\mu W$ at a location of $2.5m$ when loading was applied at $19Hz$. The highest output at a loading of $3Hz$ was found to be $0.752\mu W$, occurring at a location of $0.5m$. When loading is applied away from the natural frequencies of the structure, the power output decreases substantially (Fig. 6(b)). It was found that for loading frequencies of 7, 11, 15, 23 and $27Hz$, a maximum power output of $0.105\mu W$ occurred at a loading of $23Hz$ at a location $0.5m$ along the length of the beam.

3.2 Influence of Loading Magnitude on Energy Harvesting Potential

To investigate the effect of the magnitude of loading on the energy harvesting output, loadings of $37.5N$ and $50N$ were applied to the beam. For a loading magnitude of 37.5N, all locations produced an increase in the power equal to one and a half times that of the base case and for a loading of magnitude $50N$ the power output doubled. The peak power outputs were $1.311\mu W$ and $1.736\mu W$ for loadings of $37.5N$ and $50N$ respectively, both of these occurring at a location of $2.5m$ at a loading frequency of $19Hz$ (Fig. 7(a)). For loading away from the natural frequency, there are again similar increases in the power output along the length of the beam, with similar power output profiles to that of the baseline case (Fig. 7(b)). Such increases in power outputs illustrate the dependency of power outputs on both the loading magnitude and frequency being applied to the host structure and the profiles of the energy harvested at loading frequencies close to the frequencies of the beam correspond to the positive strain profiles at the respective modes.

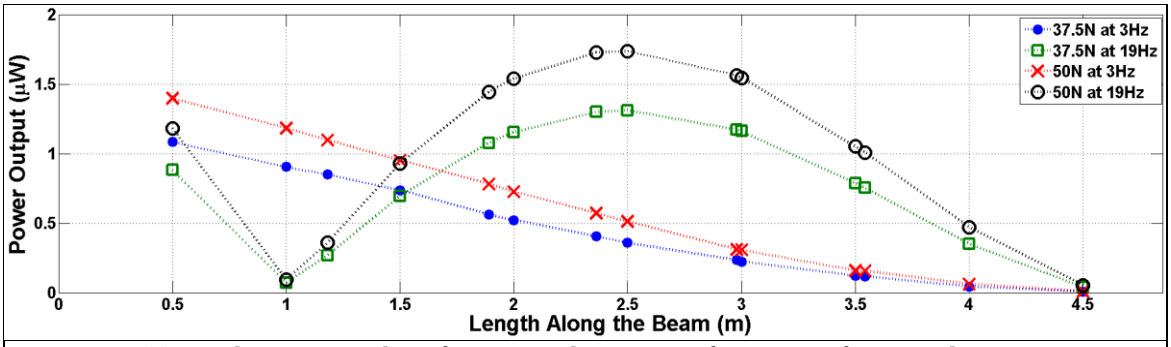

(a) Loading magnitudes of $37.5N$ and $50N$ at a frequency of $3Hz$ and $19Hz$

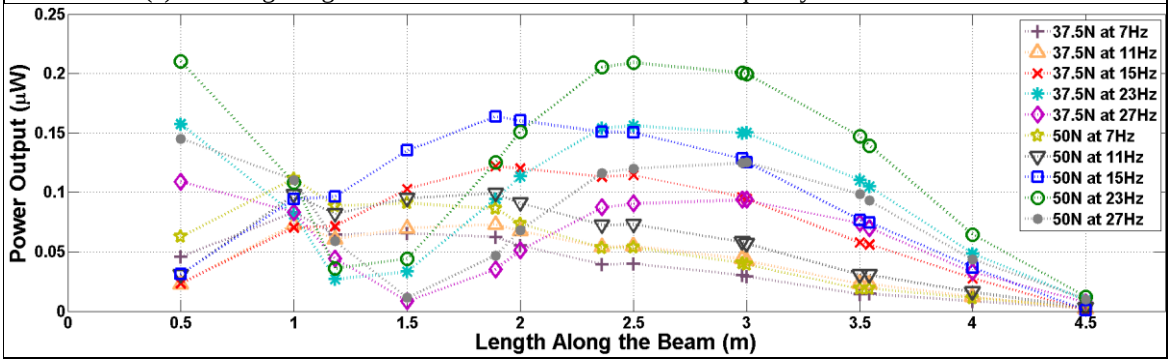

(b) Loading magnitudes of $37.5N$ and $50N$ at a frequency of $7Hz$, $11Hz$, $15Hz$, $23Hz$ and $27Hz$

Fig. 7 Effects of increased loading magnitude on energy harvesting output for $37.5N$ and $50N$ (a) L oading frequencies of $3Hz$ and $19Hz$ (b) Loading frequencies of $7Hz$, $11Hz$, $15Hz$, $23Hz$ and $27Hz$

3.3 Influence of Loading Location on Energy Harvesting Potential

The position of the loading which is applied to the cantilever beam will have an impact on the magnitude of its dynamic response and thus on the energy harvesting potential from the beam. Two additional positions of loading were investigated at a magnitude of $25N$, at the quarter-span adjacent to the base position and at the mid-span of the beam. For loadings close to the natural frequencies, there is an increase in the amount of power output along the length of the beam (Fig. 8(a)). For $3Hz$ loadings, the maximum power output for quarter-span loading was $3.935\mu W$ which increased to $13.248\mu W$ when loading was applied at the mid-span. For loading away from the natural frequencies, loading at the quarter-span provided a greater magnitude in energy harvested when compared to matching loads applied at $0.5m$ from the fixed position., while mid-span loadings generating the highest power of the cases considered (Fig. 8(b)).

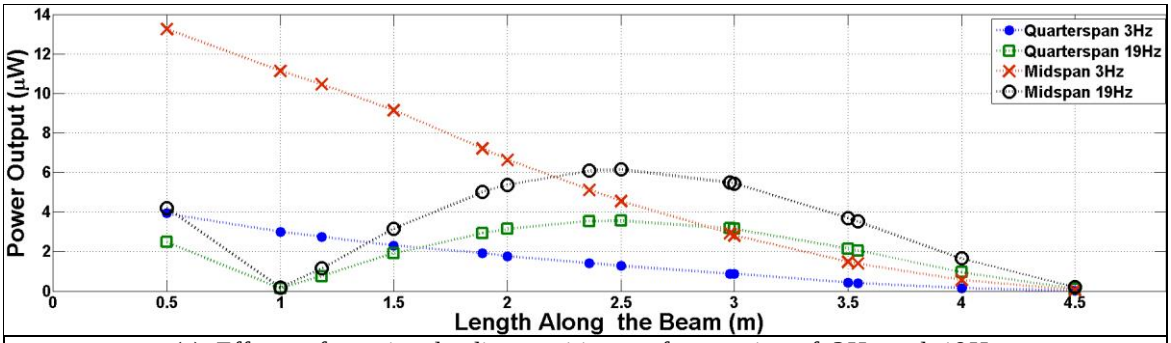

(a) Effects of varying loading position at frequencies of $3Hz$ and $19Hz$

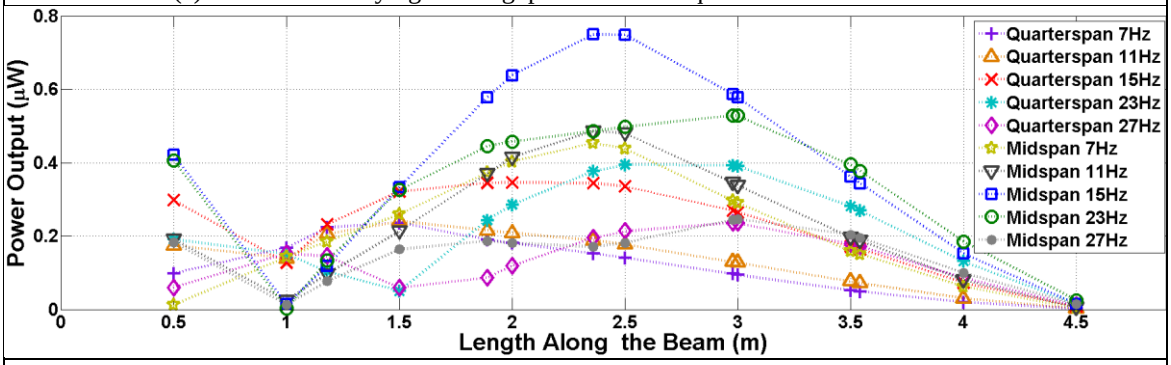

(b) Effects of varying loading position at frequencies of $7Hz$, $11Hz$, $15Hz$, $23Hz$ and $27Hz$

Fig. 8 Effects of varying loading position on energy harvesting output for loading frequencies of (a) Loading frequencies of $3Hz$ and $19Hz$ (b) Loading frequencies of $7Hz$, $11Hz$, $15Hz$, $23Hz$ and $27Hz$

4 Application of Energy Harvesting for Damage Detection

4.1 Damage Detection using Energy Harvesting Potential

For applications of damage detection using energy harvesting devices, the feasibility of using the variance in the energy harvesting potential of the devices from the structure due to the introduction and evolution of damage was subsequently investigated. Two approaches are presented here in this

regard, the first using the energy harvesting output and the second using a normalised mean for each energy harvesting device. For the second approach, a damage index based upon the comparison of the energy harvested from the healthy and damaged structure was utilised. The energy harvesting damage index (EHDI) was determined through:

$$EHDI = \frac{P_{DM}}{P_{BM}} = \frac{\left(\sqrt{\frac{1}{T_1}\int_0^{T_1} v_{DM}{}^2(t)dt}\right)^2}{\left(\sqrt{\frac{1}{T_2}\int_0^{T_2} v_{BM}{}^2(t)dt}\right)^2} \tag{10}$$

Where P_{DM} and v_{DM} are the power and voltage output from the damaged model respectively and P_{BM} and v_{BM} are the power and voltage output from the baseline model, i.e. the undamaged model. To investigate the two approaches, damage of increasing severity was introduced to the model, with damage at a location of $1.89m$ along the length of the beam being applied in the form of loss of section, as described in Section 2.3, with damage ranging from 10% to 40%. For the section loss of 10%, the flexural rigidity of the damaged elements decreases to $1.082 \times 10^5 Nm^2$ from an undamaged value of $1.219 \times 10^5 Nm^2$. As the damage magnitude increases, with a further section loss of 10%, a decrease of $1.37 \times 10^4 Nm^2$, is applied successively for each of the damage steps considered to a maximum damage of 40%. The structure was subjected to loadings of magnitude and frequency of $25N$ and $19Hz$ for each damage model and the compared to the counterpart undamaged, baseline model.

4.2 Detection of Damage Presence and Magnitude

For each of the four cases of damage, the amount of energy harvested at each device location was found to vary. The location of damage resulted in the largest variance in energy output, with an increase from $0.722\mu W$ for the baseline model to $0.803\mu W$ for 10% damage, and increasing with the evolution of damage magnitude up to a maximum of $1.21\mu W$ for 40% damage (Fig. 9(a)). Using the EHDI method, it a similar trend appears with the location of damage showing the greatest increase from 1.0 for the baseline condition, to 1.11 for 10% damage severity, up to a maximum of 1.676 for 40% damage (Fig. 9(b)). While all other device locations registered some degree of change, it is the location of damage which was found to have the largest change in power output and the largest EHDI.

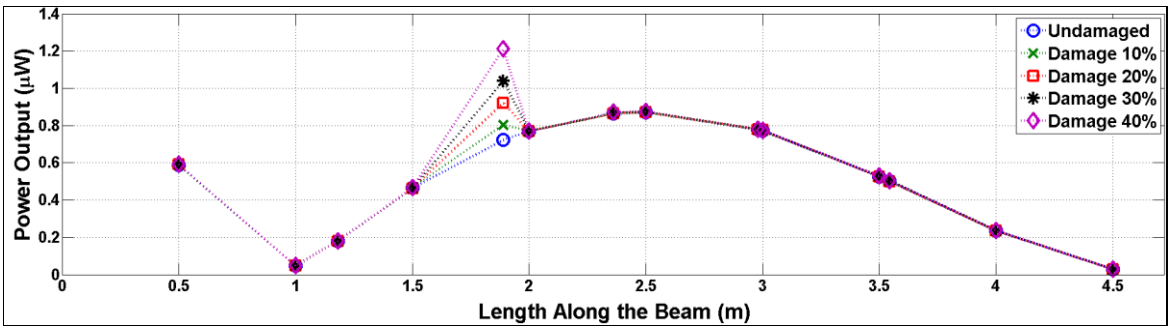

(a) Effects of introduction and evolution of damage on energy harvesting potential

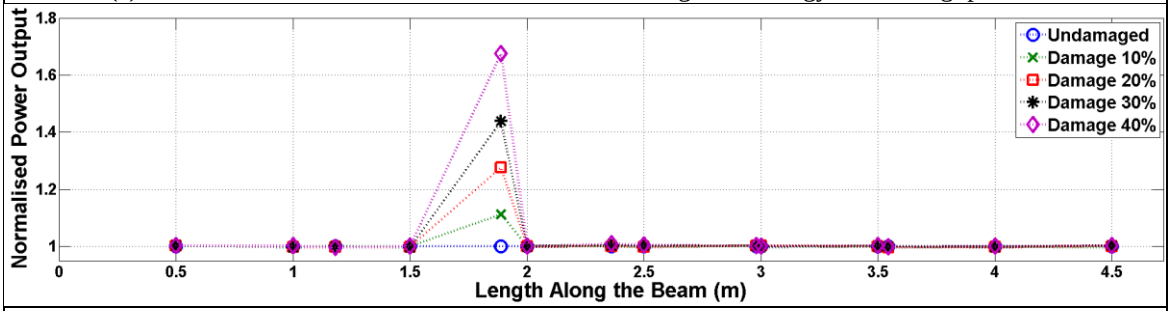

(b) Energy harvesting damage index (EHDI) for one position of damage

Fig. 9 Energy harvesting potential with the introduction of damage (a) Power output for different damage cases (b) Energy harvesting damage index (EHDI) for one position of damage for damages ranging from 10% to 40%

4.3 Multiple Locations of Damage with Increasing Magnitude

The ability of the energy harvesting devices to detect multiple locations of damage was subsequently investigated. In addition to damage at 1.89m from the base, a second position of damage was introduced, at a location 2.98m. As with the singular location of damage, damage evolution was considered with the severity of damage being considered ranging from 10% to 40%. It was found that the greatest change in the power output occurred at both locations of damage when comparing all energy harvesting devices, with the two locations of damage being identified and the evolution of damage being detected for the four damage models considered (Fig.10(a)). The EHDI illustrates the ability of an array of energy harvesting devices to detection the locations and severity of damage, with both damage locations being identifiable for each damage case and the increasing severity of the damage being detected (Fig. 10(b)).

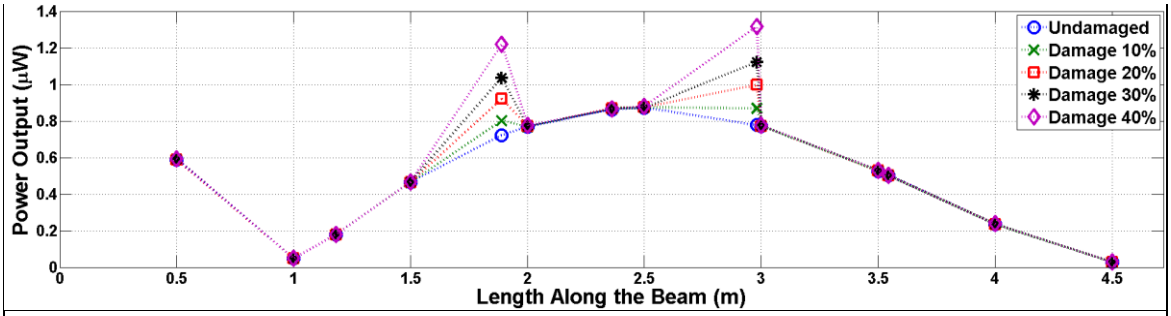

(a) Effects of introduction and evolution of damage at two locations on energy harvesting potential

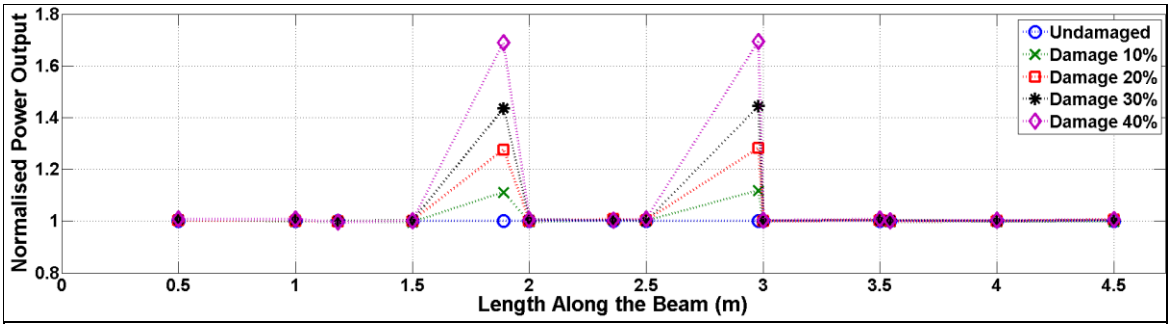

(b) Energy harvesting damage index (EHDI) for two positions of damage

Fig. 10 Energy harvesting potential with damage at two locations along the length of the beam (a) Power output for different damage cases (b) Energy harvesting damage index (EHDI) for two positions of damage

4.4 Discussion on Application of Energy Harvesting for Damage Detection

It has been presented that the location and frequency at which forced vibrations are applied to the structure can significantly affect the energy harvesting output from the structure. Upon the integration of energy harvesters with the host structure, baseline power outputs must first be established for a healthy structure to achieve further applications using power output approaches. Once these baseline power outputs have been established along the length of the structure, deviations from the normalised based under similar loading conditions at a given location can indicate a change in the integrity of the structure due to damage. By monitoring such deviations through the EHDI approach., sharp deviations over a short time period indicate a fast damage evolution, whist deviations over a longer time period indicate a gradual evolution of damage. The normalisation of the power generated by the harvesters, as required for the EHDI, is comparable to the operations if the energy harvesters were to be connected to a storage circuit for the power of wireless sensor nodes (Boyle et al. 2011). For wake-up sensing nodes, the time durations between the transmissions is dependent on a threshold storage quantity being achieved (Park and Chou 2006) and therefore these transmissions can be calibrated to the energy harvested from the host structure and used for the EHDI method for damage detection. The effect of damage on the entire global structure is similarly important when considering harvesters located at distances away from the damage. Very localised damage, as considered in this study, can be difficult to detect at locations away from the damage as its influence on the global structure is limited and therefore a finer array of devices is required, as would be the case with other sensing methodologies.

5. Energy Harvesting as an Indicator for Control of Pipeline Structure

The control of vibrations for civil structures is of significant importance in relation to adverse and extreme excitation responses. Relevant structures in this relation include high-rise buildings and bridges in earthquake prone locations (Arrigan et al. 2011). Smart materials like piezoelectric energy harvesters have been employed for damping (Hagood and Flotow 1991), but are usually not appropriate for structural damping of civil infrastructure elements due to the overall size involved. Such elements most often require the addition of active or semi-active control systems to achieve effective vibration suppression (Casciati et al. 2012), but the question arises as to the potential for using the power output of the harvester as an indicator for control. The

indicator can provide the level of success or efficiency obtained by a deployed control device, but more importantly can be used to understand the level of detuning that might have taken place for a passive vibration control device like a Tuned Mass Damper (TMD). Additionally, the level of control estimated from energy harvesting has the potential to be used for online adaptation of semi-active vibration control devices. However, for an energy harvester to be used for this purposes, experimental evidence must be present that demonstrates the sensitivity of the harvesting response to such changes.

5.1 Introduction of Tuned Mass Damper for Vibration Control

To investigate the ability of energy harvesting devices to act as indicators for control, the influence of the coupling of a TMD to the primary structure was determined, with a combined dynamical system as described in Section 2.2 being considered. The TMD device was modelled so as to match the second mode of the pipe, with a natural frequency of 19.237Hz. The influence of different mass magnitudes for the TMD was investigated, with mass ratios of 0.005, 0.01, 0.02 and 0.04 between the TMD's and the overall mass of the structure being considered in this regard.

The TMD was applied to the beam modelled as spring-mass beam element, with a constant damping ratio of 2% considered for all cases for both the TMD and the structure, applied at the mid-span. With the increasing mass of the damper being considered, the stiffness of the spring was varied in each case so as to match the designated frequency to which it is being optimised. The influence on the beam response due to the TMD is illustrated through a frequency response function (FRF), normalised against the beam model with no TMD attached (Fig. 11).

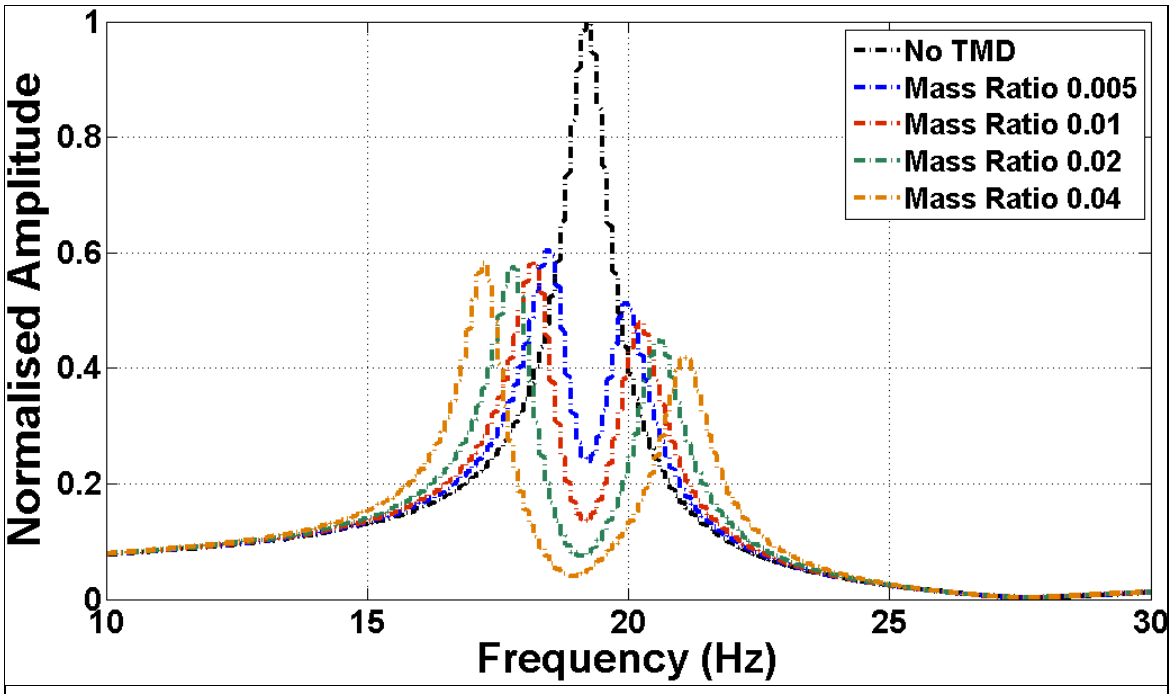

Fig. 11 Influence of TMD with varying mass ratios on natural frequency of host structure

5.2 Control Indicators Through Energy Harvesting Devices

For all TMD cases considered, the influence of the addition of control of varying magnitudes was assessed for each of the energy harvesting locations. It was found that the voltage generated at each located was reduced with the introduction of the TMD to the host structure compared against the structure without control, and continued to be reduced with increased levels of control. This is due to the damping of the vibrational response of the host structure due to the TMD and this subsequently results in a decreased power output from the coupled energy harvesting devices. An example voltage response for an energy harvesting device with the introduction of a TMD and increase in mass is illustrated in Fig. 12. With no control, the voltage response was $0.882 Vrms$ and with the introduction a TMD of mass-ratio 0.005 the voltage response was reduced to $0.261 Vrms$. With the increased control through the increase in the mass-ration to 0.01, the voltage output was further reduced to $0.156 Vrms$.

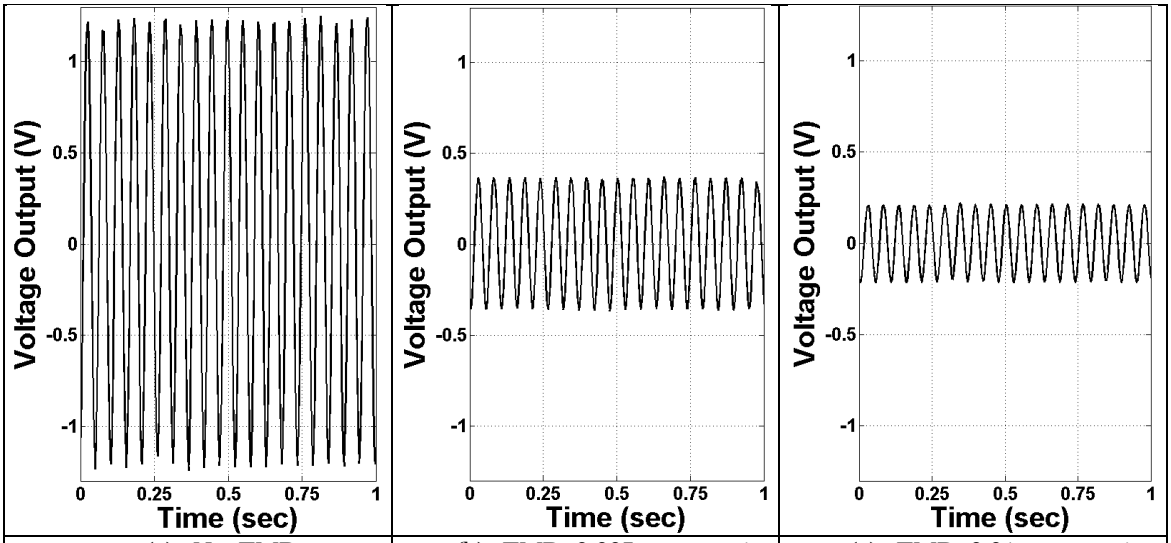

(a) No TMD (b) TMD 0.005 mass ratio (c) TMD 0.01 mass ratio

Fig. 12 Ability of energy harvesting devices to act as control indicators with voltage outputs for (a) no TMD (b) TMD with mass ratio of 0.005 (c) TMD with mass ratio of 0.01

When considering energy harvesters along the length of the beam, there is a drop in the power output at all locations from the baseline case with the introduction of the TMD. This decrease in power output from the harvesters is apparent even with the introduction of TMD with a comparatively low mass ratio between that of the TMD and the host structure of 0.005. It was found that without control, the maximum power output was $0.872 \mu W$ at a location of $2.5m$ and that this decreased to $0.258 \mu W$ when the TMD was introduced (Fig. 13). With increased control, through an increase in the mass-ratio, the amount of harvested energy further decreased at all points, with mass-ratios of 0.01 and 0.02, the power output was further reduced to $0.152 \mu W$ and $0.090 \mu W$. This trend is repeated at all locations, with reductions in power outputs with increased vibration control through the introduction of TMD's of increased mass ratios. The TMD with the highest level of control, that of mass-ratio of 0.04 resulted in a power output of $0.057 \mu W$, or a 93.5% decrease when compared to the uncontrolled structure.

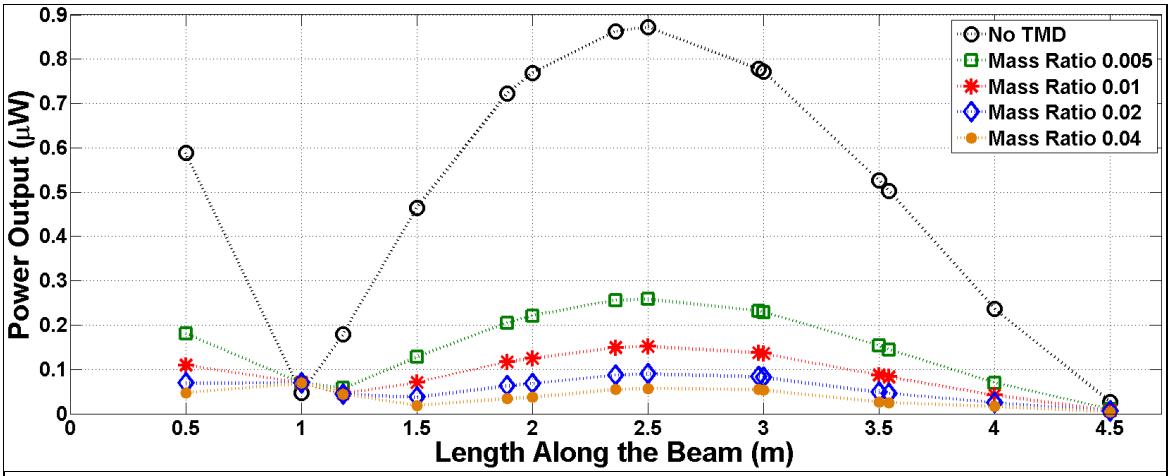

Fig. 13 Ability of energy harvesting devices to act as control indicators through variations in power output for energy harvesters with TMD's of increased mass ratio

5.3 Discussion on Energy Harvesting as an Indicator

As illustrated, the influence of introducing a control mechanism to the host structure has a significant impact on the voltage and, consequently, power output from the energy harvesting devices. Through appropriate benchmarking, as with the damage detection, thresholds for the power output from the energy harvesting array can be established about the requirement for the introduction of a control mechanism to host structure. When monitoring the power output of the energy harvesters, should the power output from the array of devices exceed the threshold markers established, the requirement for the introduction of vibration suppression is signalled. Upon the introduction of such control mechanisms, the effectiveness of the vibration control on the host structure can be monitored again through the power output from the energy harvesting array. Determining markers for the effectiveness of the control mechanism being introduced to the host structure allows for critical indicators, such as detuning, to be established and ensures the control mechanisms are sufficient (Rana and Soong 1998). Furthermore, such control indicator applications can be combined with damage detection, as if there is an increase along the length of the structure in the power output and a location registers a deviation from the normalised baseline not in keeping with its counterpart, it may indicate both the existence of damage and the requirement for vibration control to be implemented.

6. Experimental Analysis

To establish the idea of using energy harvesting for damage detection and level of vibration control, an experiment is carried out in the laboratory on a cantilever pipe structure with damage and where the vibration is suppressed due to the presence of a TMD. The experimental setup and results are detailed in the subsequent sections.

6.1 Experimental Setup

For the experimental analysis, a cantilever pipe structure with similar dimensional and material properties as those used for the theoretical analysis was chosen as the host structure. The pipe structure was restrained at its fixed end by means of a base plate bolted to a rigid structure (Fig. 14(a)). A second support, in the vertical plane so as to provide a support against gravity, was applied near its free end and only allowed movement of the pipe in a singular plane, perpendicular to the auxiliary support. The beam had two locations of damage, the nature of which consisted of two open cracks at each location on opposite sides of the pipe. At location one, a distance of 1.89m from the base, the two cracks corresponded to a 21.3% section loss, while at location two, 2.98m from the base, the two cracks result in a 15.4% section loss. The excitation of the pipe structure was provided using a spring-mass single degree of freedom (SDOF) system, acting along a linear track fastened to the pipe. The system consisted of a DC motor, with a mass affixed to the rotational shaft, which was attached to the pipe by means of a compression spring (Fig. 14(b)). The combined mass of the motor and rider were 0.32kg and the stiffness of the spring was 4027.044Nm^2. Through the control of the voltage being applied to the motor, the frequency of the loading to be regulated.

(a) Experimental cantilever pipe structure

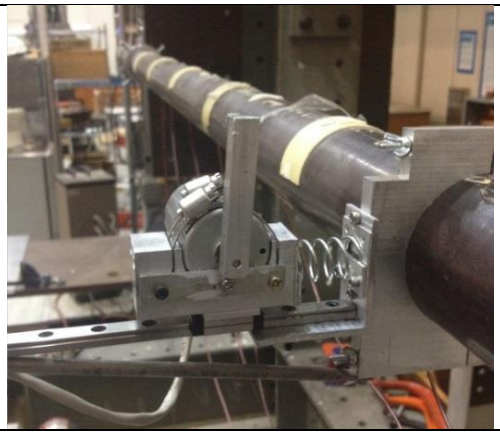

(b) SDOF excitation device

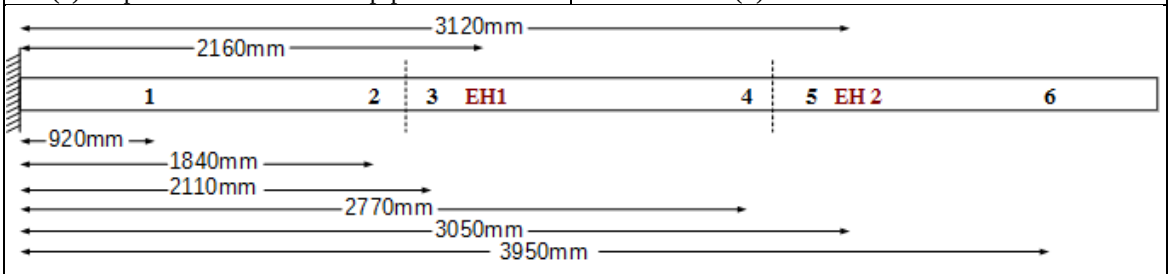

(c) Location of strain gauges and energy harvesters along the length of the beam with damage represented by dashed lines

Fig. 14 Experimental setup including (a) Cantilever pipe structure attached to rigid frame (b) Image of excitation SDOF system (c) Location of strain gauges and energy harvesters and locations of damage

Data was collected at a total of eight locations along the length of the pipe, using a combination of strain gauges and energy harvesters. There were a total of six strain gauge positions along the length of the beam, marked locations 1 to 6 (Fig. 14(c)), with data acquisition being acquired using NI 9237 strain input 398 modules, NI 9234 analogue input modules and a DAQ 9178 chassis at a sampling rate of 2kHz. Two energy harvesting patches, labelled EH1 and EH2, were placed at locations 2.16m and 3.12m from the base respectively. The energy harvesters consisted of Midé PA16N piezoelectric patches, a feature of which is some flexibility in the material and allowed for the patch to align with the curvature of the pipe. The voltage output from the energy harvesters was recorded using a Tektronix TDS2024C digital storage oscilloscope, at a sampling rate of 1kHz. Loadings from the SDOF exciter were applied at different excitation frequencies at three locations as that of the theoretical study, 0.5m from the base, the quarter-span adjacent to the base and the mid-span. The loading frequencies were applied at two bandwidths at each location, of between 13Hz and 15Hz and of between 18Hz and 22Hz, with the strain and voltage response recorded for each.

6.2 Experimental Results

For each of the loadings being applied to the host experimental structure, the strain response as measured by the array of strain sensors was obtained and compared against the experimental output from the energy harvesting devices. The sinusoidal nature of the excitation is evident in strain output, as illustrated by a typical strain output for loading of frequency 14.43Hz located at a position of 0.5m from fixed position (Fig.15(a)). It was observed that the two strain gauges which resulted in the highest strain responses, Gauge 3 and Gauge 4, were located closest to the midpoint of the cantilever structure and located adjacent to the locations of damage. The lowest strain output was from Gauge 6, located closest to the free end of the beam. The corresponding voltage response from the two energy harvesters were found to have a similar sinusoidal waveform as that from the strain gauges (Fig. 15(b)), with EH1 measuring a higher voltage output when compared to its counterpart EH2.

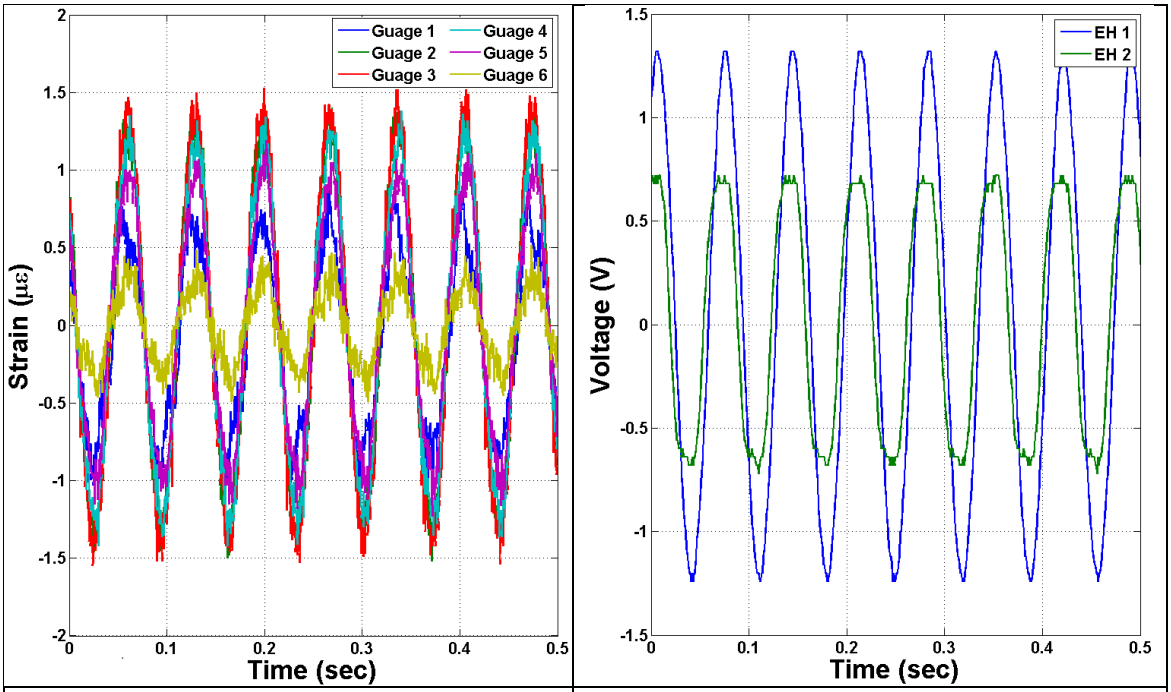

(a) Strain output (b) Voltage output

Fig. 15 A typical experimental response from (a) Strain gauges and (b) Energy harvesting devices

The first location chosen for the excitation of the experimental beam by the SDOF system was a position of $0.5m$ from the fixed end of the beam. An excitation frequency bandwidth below the second mode of the beam was applied to beam, ranging from $13.5Hz$ to $14.4Hz$, and the strain and voltage response for each obtained, with the peak magnitudes of the strain gauges at each location compared against the root mean square of the voltage. It was found that with increased loading frequency there was an increase in the magnitude both for the strain (Fig. 16(a)) and voltage (Fig. 16(b)) response. A loading frequency of $14.40Hz$ provided the highest magnitude for both strain and voltage output, with peak amplitude of $13.48\mu\varepsilon$ from Gauge 3 and $0.746V$ from EH1. For every excitation frequency considered, Gauge 3 measured the highest amplitude strain response, due to its location near the midpoint of the structure and being adjacent to the location of damage, whilst Gauge 6 measured the lowest strain response, due to its location being in the nearest to the free end of the pipe structure. When comparing the voltage response, EH1 was consistently higher than EH2

at each loading frequency.

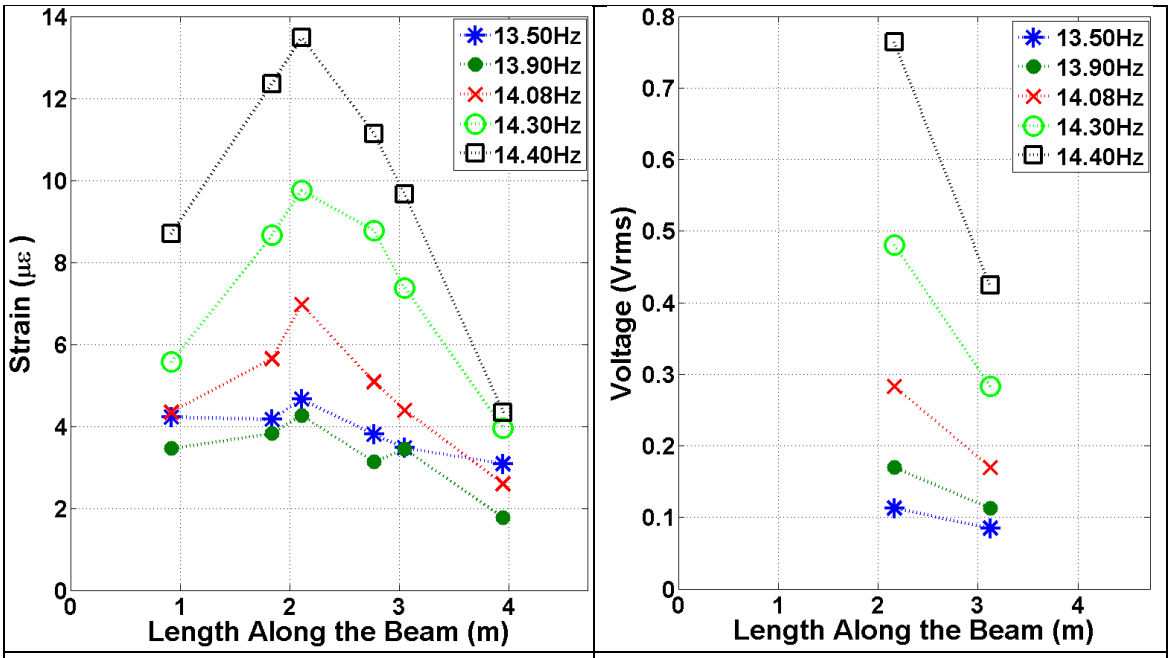

(a) Strain output (b) Voltage output

Fig. 16 Response for loading of frequency 13.5*Hz* to 14.4*Hz* at a location of 0.5*m* from fixed end with (a) Strain output and (b) Voltage output

Loading at the location of the 0.5m from the fixed end of the beam was again investigated, but with a frequency of loading above that of the second mode of the host structure. The bandwidth of loading chosen ranged between 18.80*Hz* and 20.20*Hz*, with an intermediate loading of 19.40*Hz* also being applied. Again, the loading frequency which produced the largest strain response from the array was that which was closest to the second mode of the beam, in this case 18.80Hz, with 6.74$\mu\varepsilon$ being the maximum strain response, measured by Gauge 3 (Fig. 17(a)). As the loading frequency moves away from the second mode of the beam, the strain response is seen to decrease along the length of the strain gauge array, with the lowest strain response being from a loading frequency of 20.20*Hz*., with Gauge 4 measuring a peak strain of 4.42$\mu\varepsilon$. It was found that as loading moves away from the second mode, the voltage output of the two energy harvesters similarly decreased, with EH1 decreasing from 0.125V at a loading frequency of 18.80Hz, to a voltage output of 0.060V at a loading frequency of 20.20Hz (Fig. 17(b)). As was seen for loadings in the first frequency bandwidth, EH1 produced a higher voltage response for the three loading frequencies investigated when compared to EH2. A summary of the strain and voltage outputs for excitation at frequencies above and below the second mode at a location of 0.5*m* from the fixed position are presented in Table 4.

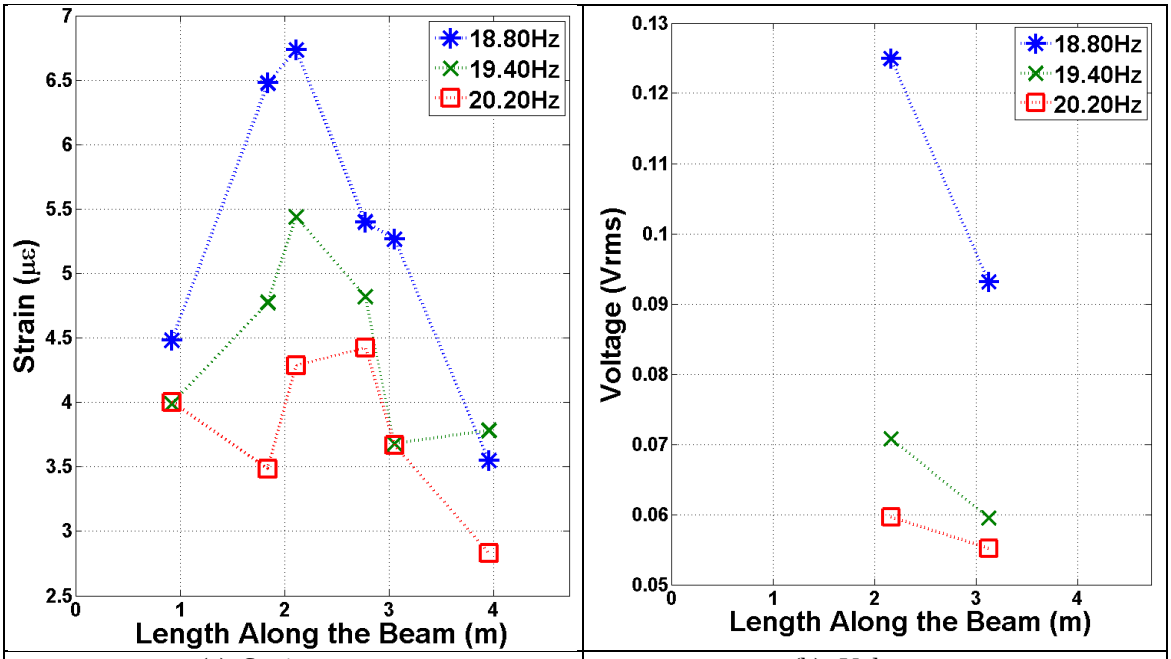

(a) Strain output (b) Voltage output

Fig. 17 Response for loadings at 0.5m from base at 18.8*Hz* to 20.2*Hz* with (a) Strain output and (b) Voltage output

Table 4. Strain and voltage responses for loading at 0.5m from fixed end of experimental beam.

Loading Frequency (Hz)	Strain (με)						Voltage (Vrms)	
	Gauge 1	Gauge 2	Gauge 3	Gauge 4	Gauge 5	Gauge 6	EH1	EH2
13.50	4.224	4.168	4.657	3.804	3.477	3.088	0.113	0.085
13.90	3.461	3.825	4.260	3.130	3.438	1.779	0.170	0.113
14.08	4.340	5.648	6.967	5.091	4.392	2.598	0.283	0.170
14.30	5.574	8.655	8.746	8.779	7.365	3.961	0.481	0.283
14.40	8.694	12.349	13.482	11.144	9.665	4.341	0.764	0.424
18.80	4.482	6.477	6.735	5.399	5.266	3.550	0.125	0.093
19.40	3.987	4.774	5.437	4.821	3.680	3.784	0.071	0.059
20.20	4.000	3.487	4.284	4.420	3.665	2.828	0.060	0.055

6.3 Influence of Loading Location on Energy Harvesting Outputs

The influence of different positions of loadings on the energy harvesting and strain outputs were subsequently investigated for the experimental beam. In this regard, loadings were applied at the quarter-span and the mid-span, with frequencies bandwidths above and below the second mode of the beam. For loading frequencies below the second mode, four frequencies were applied at the quarter-span of the beam ranging from 13.53*Hz* to 14.22*Hz* and three loading frequencies were

applied at the mid-span, ranging from 13.37Hz to 14.10Hz. It was found that, as with the loadings at the 0.5m from fixed end location, the loading frequency that produced the highest voltage and strain response was that closest to the second mode of the beam, with a reduction in magnitudes of responses at frequencies away from the second mode (Fig. 18). It was found that the peak strain response was found at Gauge 3 for both loading locations, with a maximum strain of 30.56$\mu\varepsilon$ at the quarter-span at a loading frequency of 14.22Hz (Fig. 18(a)) and again for mid-span loadings, with 38.28$\mu\varepsilon$ measured at a loading frequency of 14.10Hz (Fig. 18(c)). For both locations, EH1 produced a higher voltage output when compared to EH2, with a voltage output of 1.98V measured at the quarter-span for loading of 14.22Hz (Fig. 18(b)) and a voltage output of 2.32V measured for mid-span loadings at a frequency of 14.10Hz (Fig. 18(d)). Of note is that locations of loadings away from the fixed end of the beam result in higher response magnitudes and the shapes of the strain responses both for the quarter-span and mid-span loadings have a similar profile as that of the theoretical voltage outputs obtained from the theoretical study presented in Section 3 of this study.

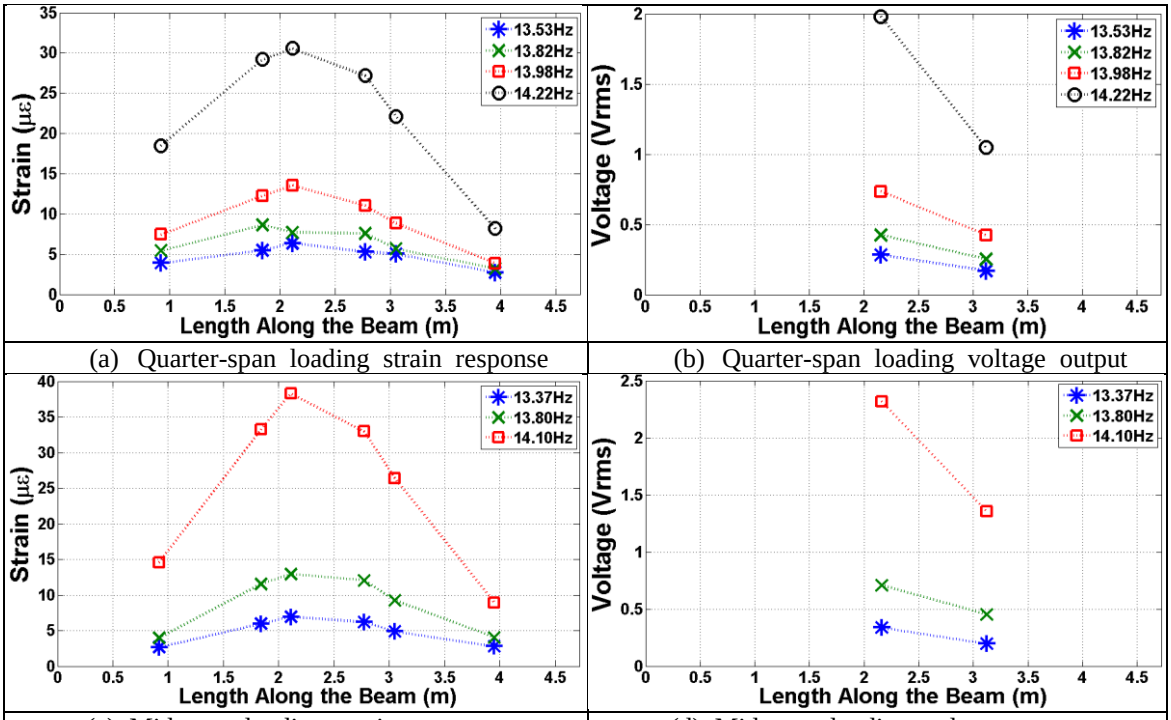

(a) Quarter-span loading strain response

(b) Quarter-span loading voltage output

(c) Mid-span loading strain response

(d) Mid-span loading voltage output

Fig. 18 Response for loading of frequencies 13.37Hz to 14.22Hz with (a) Quarter-span loading strain output (c) Quarter-span loading voltage output (c) Mid-span loading strain response and (d) Mid-span loading voltage output

Subsequent to this, loadings with a frequency bandwidth above the second mode of the experimental pipe structure were subsequently applied at the quarter-span and mid-span of the beam. It was found that at both locations the loadings with a frequency nearest the second mode again produced the highest voltage and strain responses, when compared to frequencies away from the second mode (Fig. 19). The maximum strain and voltage response for loading at the quarter-span was found to occur at Gauge 3 and EH1 at a loading frequency of 18.82Hz, with a measured output of 11.79$\mu\varepsilon$ (Fig. 19(a)) and 0.43V (Fig. 19(b)), respectively. This was similar for loadings at the mid-

span of the beam, with Gauge 3 measuring the highest strain response at a frequency of loading of 19.50*Hz*, with a measured response of 8.58$\mu\varepsilon$ (Fig. 19(c)). The maximum voltage output for the energy harvesters for mid-span loadings for frequencies above the second mode of the beam was produced by EH1 at a loading frequency of 19.50Hz, with a voltage output of 0.34V compared against an output from EH2 of 0.26V at the same loadings (Fig.19(d)).

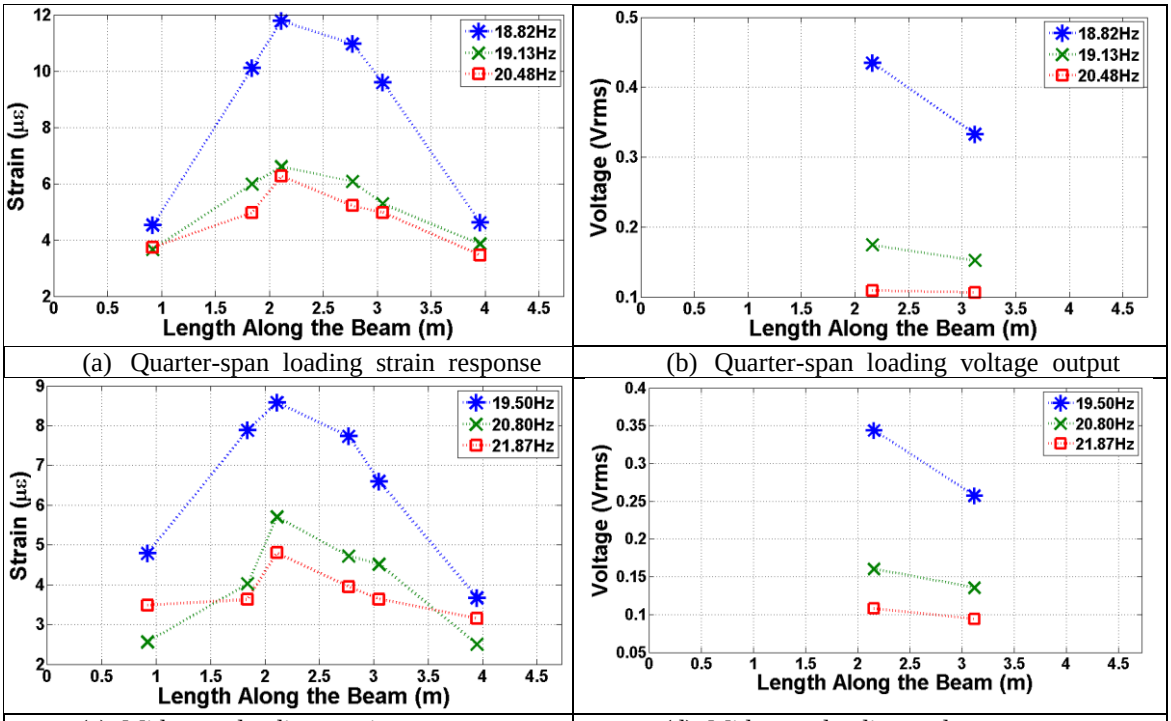

(a) Quarter-span loading strain response

(b) Quarter-span loading voltage output

(c) Mid-span loading strain response

(d) Mid-span loading voltage output

Fig. 19 Response for loadings between 18.82*Hz* to 21.87*Hz* with (a) Quarter-span loading strain output (b) Quarter-span loading voltage output (c) Mid-span loading strain response and (d) Mid-span loading voltage output

6.4 Discussion on Experimental Results

It was observed that the response from loading at frequencies between 13*Hz* and 15*Hz*, i.e. below the second mode of the beam, resulted in a greater response in both strain and voltage output when compared to loadings at frequencies of 18*Hz* and 22*Hz*, i.e. above the second mode of the beam, for all locations of loadings considered as part of the experimental study. This is due to the loading being purely sinusoidal in nature for the 13*Hz* and 15*Hz* bandwidth and modulated for frequencies of between 18*Hz* and 22*Hz*. The modulated loading is due to the excitation system acting simultaneously as a TMD for the loading bandwidth of 18*Hz* and 22*Hz*, resulting in a damping of the response from the beam. These effects were observed in the voltage output of the energy harvesting patches and verified by the strain sensing setup, with all strain gauges registering this beat response (Fig. 20(a)), as did the two energy harvesters (Fig. 20(d)). As loading moved away from the second mode of the host pipe structure, the magnitude of the waveforms for both the strain

and voltage output decreased and the beat waveform returned to sinusoidal (Fig. 20(b)(e)(c)(f)).

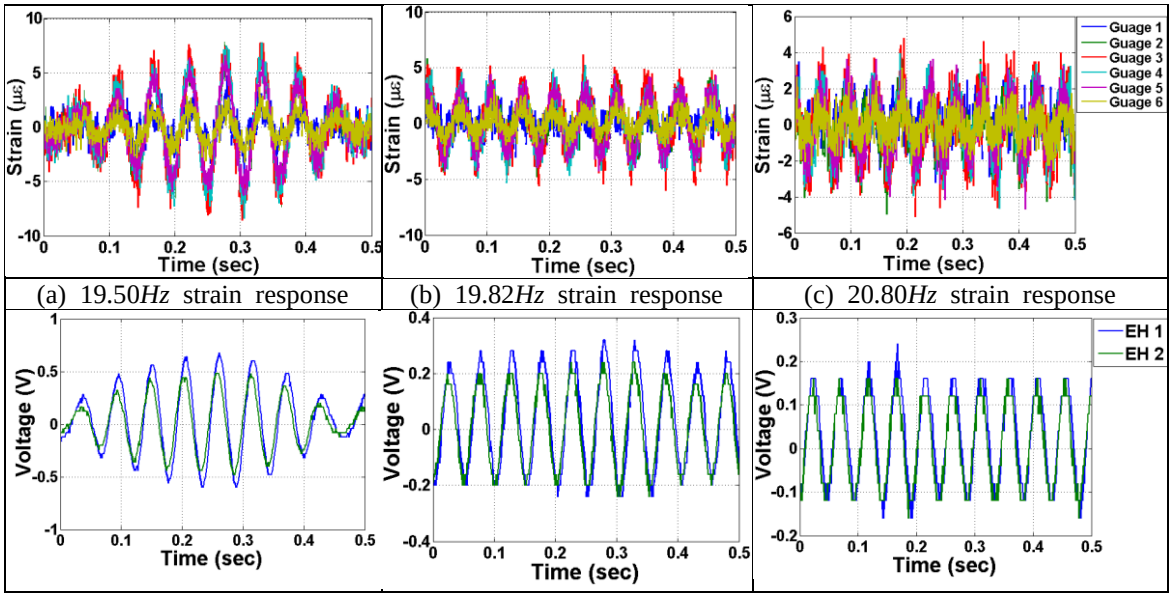

(a) 19.50*Hz* strain response (b) 19.82*Hz* strain response (c) 20.80*Hz* strain response

(d) 19.50*Hz* voltage output (e) 19.82*Hz* voltage output (f) 20.80*Hz* voltage output

Fig. 20 Experimental outputs for mid-span loadings, including strain response for loadings at (a) 19 .50*Hz* (b) 19.82*Hz* and (c) 20.80*Hz* and voltage output for (d) 19.50*Hz* (e) 19.82*Hz* and (f) 20 .80*Hz*

This modulating phenomenon is also apparent in the examination of the voltage outputs in the frequency domain, through the analysis of the output profiles using a fast Fourier transform (FFT). It is observed that for loading frequency of 19.50*Hz*, which resulted in the modulated waveform, peak amplitudes were detected at 17.207*Hz* for both EH1 and EH2, with a secondary peak detected at 19.50Hz, i.e. the excitation frequency (Fig. 21(a)). As the excitation frequency shifts away from the second mode and the modulated waveform begins to return to sinusoidal, the peak amplitude for both harvesters at a loading frequency of 18.82*Hz* was found to be at that frequency, with 17.207*Hz* still be evident but a lower amplitude (Fig. 21(b)). Finally, at a frequency of 20.80Hz, the loading frequency is again the peak amplitude for both harvesters, with 17.207Hz being notably reduced in amplitude (Fig. 21(c)).

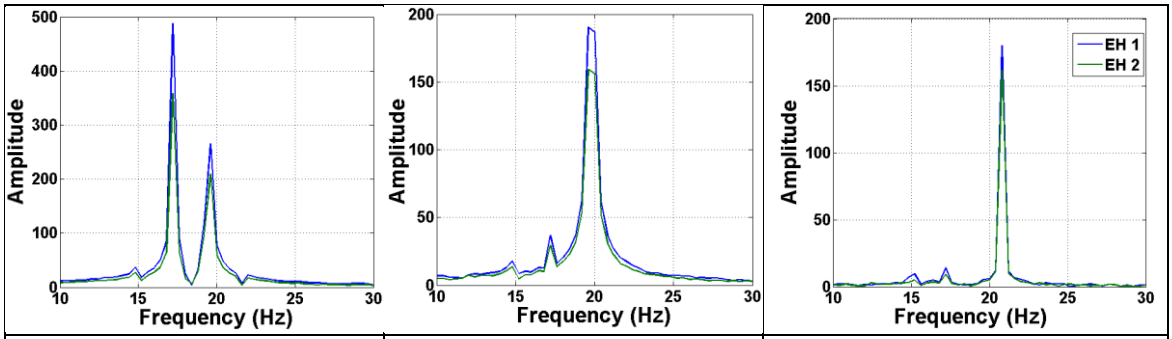

(a) 19.50*Hz* voltage frequency r (b) 19.82*Hz* voltage frequency r (c) 20.80*Hz* voltage frequency resp

esponse	esponse	onse
Fig. 21 Frequency response of energy harvesters to mid-span loadings frequencies of (a) 19.50*Hz* (b) 19.82*Hz* and (c) 20.80*Hz*		

Also of note is that the profile of the strain response along the length of the beam is comparable to the previous theoretical study. However, as damage was present in the pipe before the application of the energy harvesting devices, it is not possible to track the evolution of damage using the energy harvesters, neither through the energy harvesting out nor the EHDI. Nonetheless, it was noted that for majority of loading frequencies and positions, with two exceptions, the response of strain gauge 3, i.e. the gauge located beside the first damage location, was highest for all tests. This is in keeping with the previous numerical study which found a peak power output at the damage location.

7. Conclusions

This paper investigated the applications arising from the integration of energy harvesting devices with a host structure undergoing forced vibrations for the purposes of damage detection and indicators for control. The applications of the devices have been obtained and presented through theoretical modelling and experimental analysis of a cantilever pipe structure, under forced vibrations.

For damage detection using energy harvesting devices, a baseline model was first established and The effects of loading magnitude, frequency and position on the energy harvesting output of the devices has been presented through finite element analysis established. The analysis of the output voltage signals from an array of energy harvesters and the influence of the introduction and evolution of damage was conducted. In this regard, damage was introduced into the model and the ability of the devices to detect the damage was determined using a power output approach and an energy harvesting damage index (EHDI) approach. The ability of the energy harvesters to detect the severity of the damage and for multiple damage locations was subsequently shown. The use of power outputs from the harvester array to act as an indicator for the need for vibration control was subsequently investigated. The effects on the power output from the energy harvesting devices due to the introduction of a control mechanism in the form of a tuned mass damper (TMD) was presented. It was found that the introduction of the TMD had an impact on the power output levels from the device array, with increasing mass ratio resulting in a lower power output.

Experimental analysis was conducted on a comparable structure as that used for the theoretical analysis to verify the ability of the energy harvesting devices to act as damage detectors and indicators for control. It was found that the experimental results were similar to those obtained through the theoretical analysis and that the ability of the devices to detect damage and the requirement of control was validated. These positive results further illustrate the potential for the integration of smart energy harvesting devices with civil infrastructure systems and the wide range of applications for which they can be utilized.

Acknowledgments

The research described in this paper was financially supported by the Irish Research Council (IRC) Government of Ireland Postgraduate Scholarship Scheme under grant number GOIPG/2013/482 and by the Science Foundation Ireland (SFI) TIDA Programme under grant number 13/TIDA/I12587.

References

Amoroso, F., Pecora, R., Ciminello, M, and Concilio, A. (2015), "An original device for train bogie energy harvesting: a real application scenario", *Smart Structures and Systems*, **16**(3), 383-399.

Arrigan, J., Pakrashi, V., Basu, B. and Nagarajaiah, S. (2011). "Control of flapwise vibrations in wind turbine blades using semi-active tuned mass dampers", *Structural Control and Health Monitoring*, **18**(8), 840-851.

Arrigan, J., Huang, C., Staino, A., Basu, B. and Nagarajaiah, S. (2014). "A frequency tracking semi-active algorithm for control of edgewise vibrations in wind turbine blades", *Smart Structures and Systems*, **13**(2), 177-201.

Boyle, D., Magno, M., O'Flynn, B., Brunelli, D,. Popovici, E. and Benini, L. (2011), "Towards persistent structural health monitoring through sustainable wireless sensor networks", In: *7th International Conference Intelligent Sensors, Sensor Networks and Information Processing (ISSNIP)*,323-328.

Cahill, P., Jaksic, V., Keane, J., O'Sullivan, A., Mathewson, A., Ali, S.F. and Pakrashi, V. (2016). "Effects of road surface, vehicle, and device characteristics on energy harvesting from bridge-vehicle interactions", *Computer-Aided Civil and Infrastructure Engineering*, **31**(12), 921-935.

Cahill, P., Nullain, N.A.N., Jackson, N., Mathewson, A., Karoumi, R. and Pakrashi, V. (2014a). "Energy harvesting from train-induced response in bridges", *ASCE Journal of Bridge Engineering*, **19**(9), 04014034.

Cahill, P., O'Keefe, R., Jackson, N, Mathewson, A. and Pakrashi, V. (2014b). "Structural health monitoring of reinforced concrete beam using piezoelectric energy harvesting system", *EWSHM – 7th European Workshop on Structural Health Monitoring*, Nantes, July.

Carden, E.P. and Fanning, P. (2004). "Vibration based condition monitoring: a review". *Structural Health Monitoring*, **3**(4), 355-377.

Chen, R.L. and Wang, B.T. (2004). "The use of polyvinylidene fluoride films as sensors for the experimental modal analysis of structures", *Smart Materials and Structures*, **13**(4), 791-799.

Cheraghi, N., Zou, G.P. and Taheri, F. (2005), "Piezoelectric-based degradation assessment of a pipe using fourier and wavelet analysis". *Computer-Aided Civil and Infrastructure Engineering*, **20**(5), 369-382.

Contreras, M.T., Pasala, DTR. and Nagarajaiah, S. (2014). "Adaptive length SMA pendulum smart tuned mass damper performance in the presence of real time primary system stiffness change", *Smart Structures and Systems*, **13**(2), 219-233.

Erturk, A. (2011). "Piezoelectric energy harvesting for civil infrastructure system applications: Moving loads and surface strain fluctuations", *Journal of Intelligent Material Systems and Structures*, **22**(17), 1959-1973.

Erturk, A. and Inman, D.J. (2011). "Piezoelectric Energy Harvesting". John Wiley & Sons Ltd., Chichester, UK.

Gonzalez-Buelga, A., Clare, L.R., Cammarano, A., Neild, S.A., Burrow, S.G. and Inman, D.J. (2014), "An optimized tuned masss damper/harvester device", *Structural Control and Health Monitoring*, **21**(8), 1154-1169.

Hagood, N. W. and von Flotow, A. (1991), "Damping of structural vibrations with piezoelectric materials and passive electrical networks", *Journal of Sound and Vibration*, **146**(2), 243-268.

IEEE (1988), "Standard on Piezoelectricity ANSI/IEEE Std. 176-1987", The Institute of Electrical and Electronics Engineers, New York.

Jang, D.D., Jung, H.J. and Nagarajaiah, S. (2014), "Active mass damper system using time delay control algorithm for building structure with unknown dynamics", **13**(2), 305-318.

Jaksic, V., Mandic, D.P., Ryan, K., Basu, B. and Pakrashi V. (2016). "A Comprehensive Study of the Delay Vector Variance Method for Quantification of Nonlinearity in Dynamical Systems". *Royal Society Open Science*, **2**, 150493-1-24.

Jassim, Z., Ali, N., Mustapha, F. and Abdul Jalil, N. (2013). "A review on the vibration analysis for a damage occurrence of a cantilever beam", *Engineering Failure Analysis*, **31**, 442-461.

Kim, S.H., Ahn, J.H., Chung, H.M. and Kang, H.W. (2011). "Analysis of piezoelectric effects on various loading conditions for energy harvesting in a bridge system", *Sensors and Actuators A: Physical*, **167**(2), 468-483.

Marano, G.C., Sgobba, S., Greco, R. and Mezzina, M. (2008), "Robust optimum design of tuned mass dampers devices in random vibrations mitigation", *Journal of Sound and Vibration*, **313**(3-5), 472-492.
Nagarajaiah, S and Jung, H-J. (2014). "Smart tuned mass dampers: recent developments", *Smart Structures and Systems*, **13**(2), 173-176.
Nagarajaiah, S. (2009). "Adaptive passive, semiactive, smart tuned mass dampers: identification and control using empirical mode decomposition, hilbert transform, and short-term Fourier transform", *Structural Control and Health Monitoring*, **16**(7-8), 800-841.
Nahvi, H. and Jabbari, M. (2005). "Crack detection in beams using experimental modal data and finite element model", International Journal of Mechanical Sciences, **47**(10), 1477-1497.
Pakrashi, V., Kelly, J., Harkin, J. and Farrell A. (2013). "Hurst Exponent Footprints from Activities on a Large Structural System", *Physica A*, **392**(8), 1803 – 1817.
Pakrashi V, O' Connor A and Basu B. (2007). "A Study on the Effects of Damage Models and Wavelet Bases for Damage Identification and Calibration in Beams". Computer Aided Civil and Infrastructure Engineering, 22, 555-569
Pasala., DTR and Nagarajaiah, S. (2014). "Adaptive-length pendulum smart tuned mass damper using shape-memory-alloy wire for tuning period in real time", Smart Structures and Systems, 13(2), 203-217.
Park, C and Chou, P. H. (2006), "AmbiMax: Autonomous energy harvesting platform for multi-supply wireless sensor nodes", In: *3rd Annual IEEE Communications Society on Sensor and Ad Hoc Communications and Networks*, Reston, VA, 168-177.
Park, G., Sohn, H., Farrar, C.R. and Inman, D.J. (2003). "Overview of piezoelectric impedance-based health monitoring and path forward", *The Shock and Vibration Digest*, **35**(6), 451-463.
Rabinovitch, O. and Vinson, J. (2002). "Adhesive layer effects in surface-mounted piezoelectric actuators", *Journal of Intelligent Material Systems and Structures*, **13**(11), 689-704.
Rana, R. and Soong, T. T. (1998), "Parametric study and simplified design of tuned mass dampers" *Engineering Structures*, **20**(3), 193 – 204.
Rezaei, D. and Taheri, F. (2009), "Experimental validation of a novel structural damage detection method based on empirical mode decomposition". *Smart Materials and Structures*, **18**(4), 045004.
Saadon, S. and Sidek, O. (2011), "A review of vibration-based MEMS piezoelectric energy harvesters", *Energy Conversion and Management*, **52**(1), 500-504.
Sirohi, J. and Chopra, I. (2000), "Fundamental understanding of piezoelectric strain sensors", *Journal of Intelligent Material Systems and Structures*, **11**(4), 246-257.
Sodano, H.A., Inman, D.J. and Park, G. (2004), "A review of power harvesting from vibration using piezoelectric materials", *Shock and Vibration Digest*, **36**(3), 197-206.
Song, G., Sethi, V. and Li, H.N. (2006), "Vibration control of civil structures using piezoceramic smart materials: A review", *Engineering Structures*, **28**(11), 1513-1524.
Srbinovski, B., Magno, M., Edwards Murphy, F., Pakrashi, V. and Popovici E. (2016). "An Energy Aware Adaptive Sampling Algorithm for Energy Harvesting WSN with Energy Hungry Sensors". *Sensors*, **16**(4), 448, 1-19.
Sun, C., Nagarajaiah, S. and Dick, AJ. (2014). "Family of smart tuned mass dampers with variable frequency under harmonic excitations and ground motions: closed-form evaluation", *Smart Structures and Systems*, **13**(2), 319-341
Taghvaei, M., Beck, S.B.M. and Staszewski, W.J. (2007), "Leak detection in pipeline networks using low-profile piezoceramic transducers", *Structural Control and Health Monitoring*, **14**(8), 1063-1082.